

Technical University of Crete
School of Electrical and Computer Engineering



Estimation of sparse, in the angle domain, Massive MIMO
channels

by
Pavlos Stylianos Neonakis

THESIS COMMITTEE:
Professor Athanasios P. Liavas, *Thesis Supervisor*
Professor George N. Karystinos
Professor Michael Paterakis

Contents

| | | |
|----------|---|-----------|
| 1 | Introduction | 8 |
| 1.1 | Motivation | 8 |
| 1.2 | Thesis Outline | 8 |
| 2 | Wireless Channel Models | 9 |
| 2.1 | Physical modeling of the MIMO channel | 9 |
| 2.1.1 | Line-of-Sight SIMO channel | 9 |
| 2.1.2 | Line-of-Sight MISO channel | 11 |
| 2.1.3 | Antenna arrays with only a line-of-sight (MIMO channel) | 13 |
| 2.1.4 | Geographically separated transmit antennas | 14 |
| 2.1.5 | Geographically separated receive antennas | 18 |
| 2.1.6 | Line-of-Sight MIMO channel with one reflected path | 19 |
| 2.2 | Modeling of MIMO Fading Channels | 21 |
| 2.2.1 | Basic Approach | 21 |
| 2.2.2 | MIMO Multipath Channel | 23 |
| 2.2.3 | Angular Domain Representation of Signals | 23 |
| 2.2.4 | Angular Domain Representation of MIMO Channels | 26 |
| 2.2.5 | Statistical Modeling in the Angular Domain | 27 |
| 2.3 | Sparsity structures in Massive MIMO channel | 27 |
| 2.3.1 | Massive MIMO | 27 |
| 2.3.2 | Sparsity structures | 30 |
| 3 | Problem statement | 31 |
| 3.1 | Partial Support Information | 31 |
| 3.2 | Weighted ℓ_1 minimization using Partial Support Information | 32 |
| 3.3 | Weighted ℓ_1 minimization method with different weights | 32 |
| 4 | Numerical results | 34 |
| 4.1 | Quality of the estimated CSI versus the training overhead | 34 |
| 4.2 | Comparison of simple weighted ℓ_1 minimization method to methods with different weights | 38 |
| 4.3 | Phase Transitions | 42 |

CONTENTS

| | | |
|----------|--------------------------------------|-----------|
| 5 | Conclusions & Future work | 44 |
| 5.1 | Conclusions | 44 |
| 5.2 | Future work | 44 |
| A | Proof of Equation (2.29) | 45 |
| | Bibliography | 46 |

List of Figures

| | | |
|-----|---|----|
| 2.1 | Line-of-sight channel with single transmit antenna and multiple receive antennas. The signals from the transmit antenna arrive almost in parallel at the receiving antennas. | 10 |
| 2.2 | Line-of-sight channel with multiple transmit antennas and single receive antenna. | 12 |
| 2.3 | Two geographically separated transmit antennas each with line-of-sight to a receive antenna array. | 14 |
| 2.4 | Beamforming patterns for different antenna array lengths. (Left) $L_r = 4$ and (right) $L_r = 8$. Antenna separation is fixed at half the carrier wavelength. The larger the length of the array, the narrower the beam ([4]). | 16 |
| 2.5 | Receive beamforming patterns aimed at 90° , with antenna array length $L_r = 2$ and different numbers of receive antennas n_r . Note that the beamforming pattern is always symmetrical about the $0^\circ - 180^\circ$ axis, so lobes always appear in pairs. For $n_r = 4, 6, 32$, the antenna separation $\Delta_r \leq 1/2$, and there is a single main lobe around 90° (together with its mirror image). For $n_r = 2$, $\Delta_r = 1 > 1/2$ and there is an additional pair of main lobes ([4]). | 17 |
| 2.6 | Two geographically separated receive antennas each with line of sight from a transmit antenna array. | 18 |
| 2.7 | MIMO channel with a direct path and a reflected path. | 19 |
| 2.8 | Channel is viewed as a concatenation of two channels \mathbf{H}' and \mathbf{H}'' with intermediate (virtual) relays A and B. | 21 |
| 2.9 | An illustration of the MIMO channel in the angular domain and the resolvable bins. There are a transmitter with 4 antennas ($L_t = 2$) and a receiver with 4 antennas ($L_r = 2$). Moreover, the receiver is inside a building. Also, there are a line-of-sight path (path A) and a reflected path (path B). Due to the limited resolvability of the antenna arrays, the physical paths are partitioned into resolvable bins of angular widths $1/L_r$ by $1/L_t$ | 22 |

| | | |
|------|---|----|
| 2.10 | Receive beamforming patterns of the angular basis vectors. Independent of the antenna spacing, the beamforming patterns all have the same beam widths for the main lobe, but the number of main lobes depends on the spacing. (a) Critically-spaced case (b) Sparsely-spaced case (c) Densely-spaced case([4]). | 25 |
| 2.11 | The bin \mathcal{R}_k is the set of all paths that arrive roughly in the direction of the main lobes of the beamforming pattern of $\mathbf{e}_r(k/L)$. Here $L_r = 2$ and $n_r = 4$ ([4]). | 26 |
| 2.12 | Some examples of \mathbf{H}^a . (a) Small angular spread at the transmitter. (b) Small angular spread at the receiver. (c) Small angular spreads at both the transmitter and the receiver. (d) Full angular spreads at both the transmitter and the receiver ([4]). | 28 |
| 2.13 | Some examples of \mathbf{H}^a . (a) Two clusters of scatterers, with all paths going through a single bounce. (b) Paths scattered via multiple bounces ([4]). | 29 |
| 3.1 | Illustration of partial support information ($T = \{3, 4, 5, 7\}$, $\hat{T} = \{3, 4, 5, 8\}$ and $\text{card}(T \cap \hat{T}) = \lfloor a\hat{s} \rfloor = \frac{3}{4} \cdot 4 = 3$). | 32 |
| 4.1 | Normalized mean square error versus number of measurements with $M = 100$, $s = 20$, $\hat{s} = 25$ and $\ \mathbf{e}\ _2 = 1$ | 35 |
| 4.2 | Normalized mean square error versus number of measurements with $M = 128$, $s = 25$, $\hat{s} = 32$ and $\ \mathbf{e}\ _2 = 1$ | 35 |
| 4.3 | Normalized mean square error versus number of measurements with $M = 128$, $s = 8$, $\hat{s} = 10$ and $\ \mathbf{e}\ _2 = 1$ | 36 |
| 4.4 | Normalized mean square error versus number of measurements with $M = 100$, $s = 36$, $\hat{s} = 40$ and $\ \mathbf{e}\ _2 = 1$ | 36 |
| 4.5 | NMSE versus number of measurements with $M = 100$, $s = 20$, $a = 0.8$ and $\ \mathbf{e}\ _2 = 1$ | 37 |
| 4.6 | NMSE versus number of measurements with $M = 100$, $s = 20$, $a = 0.6$ and $\ \mathbf{e}\ _2 = 1$ | 37 |
| 4.7 | NMSE versus number of measurements with $M = 100$, $s = 20$, $\hat{s} = 25$, $a = 0.6$ and $\ \mathbf{e}\ _2 = 1$ | 38 |
| 4.8 | NMSE versus number of measurements with $M = 100$, $s = 20$, $\hat{s} = 25$, $a = 0.7$ and $\ \mathbf{e}\ _2 = 1$ | 39 |
| 4.9 | NMSE versus number of measurements with $M = 100$, $s = 20$, $\hat{s} = 25$, $a = 0.8$ and $\ \mathbf{e}\ _2 = 1$ | 39 |
| 4.10 | NMSE versus number of measurements with $M = 100$, $s = 37$, $\hat{s} = 40$, $a = 0.6$ and $\ \mathbf{e}\ _2 = 1$ | 40 |
| 4.11 | NMSE versus number of measurements with $M = 100$, $s = 37$, $\hat{s} = 40$, $a = 0.75$ and $\ \mathbf{e}\ _2 = 1$ | 40 |
| 4.12 | NMSE versus number of measurements with $M = 100$, $s = 37$, $\hat{s} = 40$, $a = 0.85$ and $\ \mathbf{e}\ _2 = 1$ | 41 |
| 4.13 | NMSE versus number of measurements with $M = 100$, $s = 37$, $\hat{s} = 40$, $a = 0.9$ and $\ \mathbf{e}\ _2 = 1$ | 41 |

LIST OF FIGURES

4.14 Phase Transition with $M = 100, \hat{s} = 10, a = 0.8$ and $\|\mathbf{e}\|_2 = 0$ 42
4.15 Phase Transition with $M = 128, \hat{s} = 10, a = 0.8$ and $\|\mathbf{e}\|_2 = 10^{-3}$ 43

Abstract

One of the technologies that makes 5G different from previous generations of wireless communications systems is Massive MIMO. When we refer to Massive MIMO, we mean that there are many antennas (of the order of hundreds) at the Base Station.

Major benefits of Massive MIMO systems are the increased energy efficiency, through directional beamforming, and the increased channel capacity. In order to attain these advantages, it is crucial to have channel knowledge at the transmitter, which, in this case, requires large training overhead, due to the large number of channel coefficients.

In this Diploma thesis, we exploit the channel sparsity in the angle domain and study Massive MIMO channel estimation methods with low training overhead. First, we present an approach where channel estimation is done by the minimization of a weighted ℓ_1 norm, with weights equal to 0 and 1, using prior knowledge about the positions of the nonzero elements in the angular domain. Next, we propose an alternative, where we use different weights. We simulate these methods and we test their behavior in many case studies.

Acknowledgements

I would like to thank my supervisor Prof. Athanasios P. Liavas for his guidance throughout this work.

Also, I would like to extend my sincere thanks to Prof. George N. Karystinos and Prof. Michael Paterakis for being members of thesis committee.

Last but not least, I would like to thank my family and my friends for their support throughout my studies.

Chapter 1

Introduction

1.1 Motivation

Massive MIMO is a technology which offers significant benefits in 5G, for example, improved energy and spectral efficiency. It turns out that channel knowledge at the Base Station is very important for achieving these benefits [1], [2]. High dimensionality of the channel vectors, owing to the large number of transmit antennas, is a challenge because it leads to large training overhead. However, Massive MIMO channels are sparse in the angular domain [2]. In this thesis, we present and evaluate a 0-1 weighted ℓ_1 minimization method which exploits prior knowledge [3]. We extend this approach by introducing various weighted ℓ_1 minimizations.

1.2 Thesis Outline

This thesis is organised as follows. In Chapter 2, we present simple models of physical wireless channels. We describe MIMO fading channels and we introduce the Angular Domain Representation of MIMO channels. Further, we present Massive MIMO and the sparsity of MIMO channels in the Angular Domain.

Chapter 3 is a description of the problem which we encounter in this thesis. We provide definitions about the weighted ℓ_1 minimization method using partial support information and we introduce our proposed extension of this method.

In Chapter 4, we present numerical results concerning the performance of the methods which we referred to.

Chapter 5 presents the conclusions of this thesis and possible future work.

Chapter 2

Wireless Channel Models

2.1 Physical modeling of the MIMO channel

In this section, we study uniform linear antenna arrays (ULAs). Moreover, we assume far field and plane wave propagation.

2.1.1 Line-of-Sight SIMO channel

Let us consider a Single Input Multiple Output (SIMO) channel. In this case, there is one transmit antenna and n_r receive antennas (Figure 2.1) with only direct line-of-sight paths between the transmit and the receive antennas [4].

The channel between the transmitter and the i^{th} receive antenna has continuous-time impulse response $h_i(\tau)$ that is given by:

$$h_i(\tau) = a\delta(\tau - d_i/c), \quad i = 1, \dots, n_r, \quad (2.1)$$

where a is the attenuation of the path (assuming same a for all antennas), d_i is the distance between the transmit antenna and i^{th} receive antenna and c is the speed of light.

Considering $d_i/c \ll 1/W$, where W is the transmission bandwidth, the single-tap model can be used. So, the baseband channel gain is given by:

$$h_i = a \exp\left(-\frac{j2\pi f_c d_i}{c}\right) = a \exp\left(-\frac{j2\pi d_i}{\lambda_c}\right), \quad (2.2)$$

where f_c is the carrier frequency and λ_c is the carrier wavelength.

The channel model is given by:

$$\mathbf{y} = \mathbf{h}x + \mathbf{w}, \quad (2.3)$$

where \mathbf{y} is the received signal vector, $\mathbf{h} = [h_1 \dots h_{n_r}]^T$ is the vector of channel gains, x is the transmitted symbol and $\mathbf{w} \sim \mathcal{CN}(0, N_0 \mathbf{I}_{n_r})$ is the noise. The vector \mathbf{h} is also called the spatial signature [4], [5].

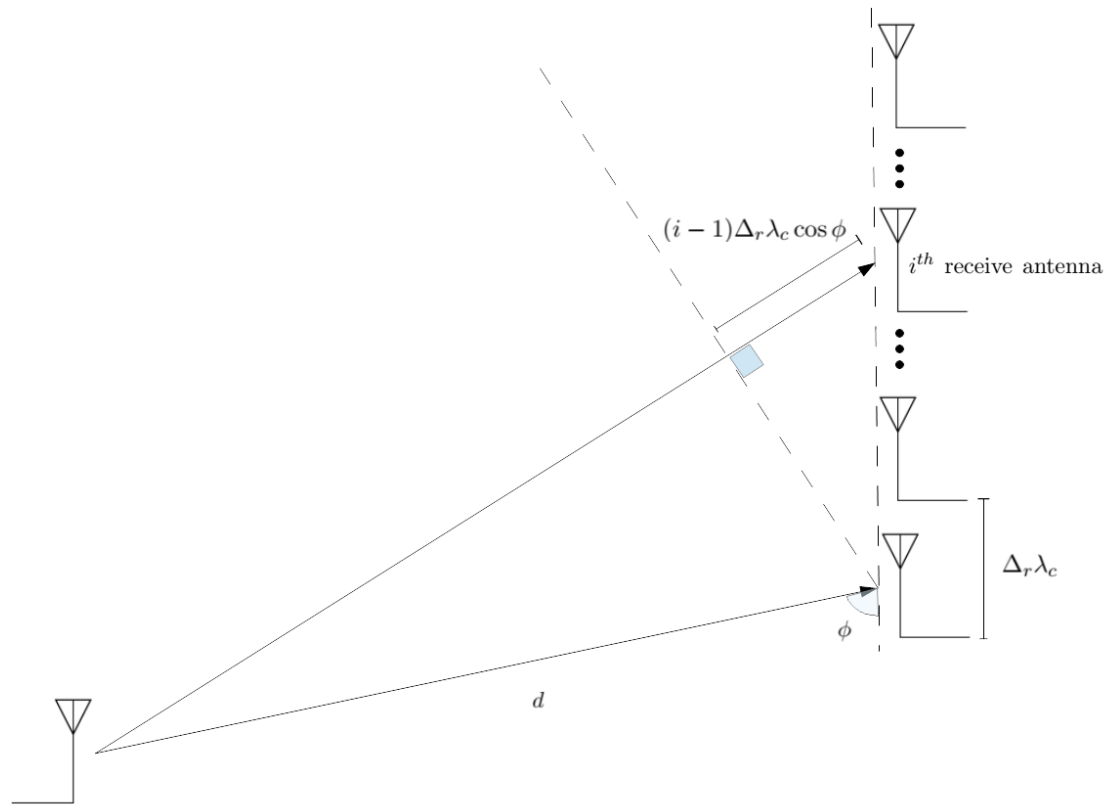


Figure 2.1: Line-of-sight channel with single transmit antenna and multiple receive antennas. The signals from the transmit antenna arrive almost in parallel at the receiving antennas.

The distance between the transmitter and the receiver is much larger than the size of the antenna array. Hence, the paths from the transmit antenna to each of the receive antennas are, to a first-order, parallel and

$$d_i \approx d + (i-1)\Delta_r \lambda_c \cos \phi, \quad i = 1, \dots, n_r, \quad (2.4)$$

where d is the distance between the antenna of transmitter and the first receive antenna, Δ_r is the receive antenna separation, normalized to the unit of the carrier wavelength, λ_c is the carrier wavelength and ϕ is the angle of incidence of the line of sight onto the receive antenna array.

So, the baseband channel gain is given by:

$$h_i = a \exp\left(-\frac{j2\pi d_i}{\lambda_c}\right) \quad (2.5)$$

$$\approx a \exp\left(-\frac{j2\pi d + j2\pi(i-1)\Delta_r \lambda_c \cos \phi}{\lambda_c}\right) \quad (2.6)$$

$$= a \exp\left(-\frac{j2\pi d}{\lambda_c}\right) \cdot \exp\left(-\frac{j2\pi(i-1)\Delta_r \lambda_c \cos \phi}{\lambda_c}\right) \quad (2.7)$$

$$= a \exp\left(-\frac{j2\pi d}{\lambda_c}\right) \cdot \exp(-j2\pi(i-1)\Delta_r \cos \phi), \quad i = 1, \dots, n_r. \quad (2.8)$$

If $\Omega := \cos \phi$, then the spatial signature \mathbf{h} is given by:

$$\mathbf{h} = a \exp\left(-\frac{j2\pi d}{\lambda_c}\right) \begin{bmatrix} 1 \\ \exp(-j2\pi\Delta_r\Omega) \\ \vdots \\ \exp(-j2\pi(n_r-1)\Delta_r\Omega) \end{bmatrix}. \quad (2.9)$$

The unit spatial signature in the directional cosine Ω is defined as:

$$\mathbf{e}_r(\Omega) := \frac{1}{\sqrt{n_r}} \begin{bmatrix} 1 \\ \exp(-j2\pi\Delta_r\Omega) \\ \vdots \\ \exp(-j2\pi(n_r-1)\Delta_r\Omega) \end{bmatrix}. \quad (2.10)$$

2.1.2 Line-of-Sight MISO channel

The Multiple Input Single Output (MISO) channel is similar to the SIMO channel, but there are n_t transmit antennas and one receive antenna (Figure 2.2). The channel model is given by:

$$y = \mathbf{h}^* \mathbf{x} + w, \quad (2.11)$$

where y is the received signal, \mathbf{h}^* is the conjugate-transpose of the vector of channel gains \mathbf{h} , \mathbf{x} is the transmitted symbol in vector form and $w \sim \mathcal{CN}(0, N_0)$ is the noise [4], [5].

The vector of channel gains \mathbf{h} is given by:

$$\mathbf{h} = a \exp\left(\frac{j2\pi d}{\lambda_c}\right) \begin{bmatrix} 1 \\ \exp(-j2\pi\Delta_t\Omega) \\ \vdots \\ \exp(-j2\pi(n_t-1)\Delta_t\Omega) \end{bmatrix}, \quad (2.12)$$

where $\Omega := \cos \phi$ (ϕ is angle of departure).

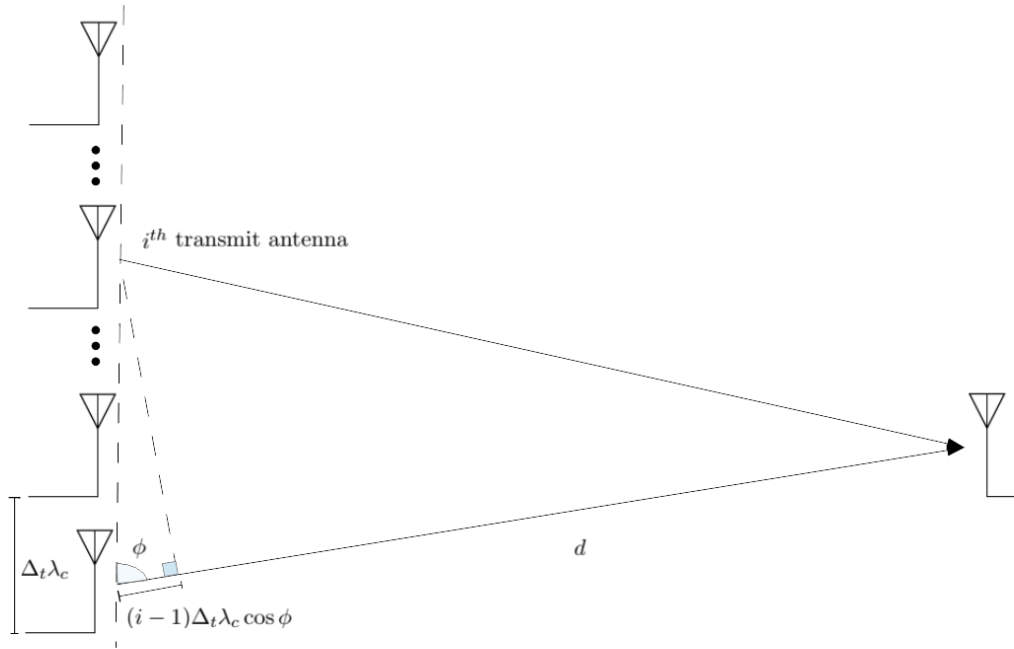


Figure 2.2: Line-of-sight channel with multiple transmit antennas and single receive antenna.

If the distance between the transmitter and the receiver is much larger than the size of the antenna array then the paths from the transmit antennas to the receive antenna are, to a first-order, parallel and

$$d_i \approx d - (i-1)\Delta_t \lambda_c \cos \phi, \quad i = 1, \dots, n_t, \quad (2.13)$$

where d is the distance between the first transmit antenna and the receive antenna, Δ_t is the normalized transmit antenna separation, normalized to the unit of the carrier wavelength λ_c .

The channel gain is

$$h_i^* = a \exp\left(-\frac{j2\pi d_i}{\lambda_c}\right) \quad (2.14)$$

$$\approx a \exp\left(-\frac{j2\pi d - j2\pi(i-1)\Delta_t \lambda_c \cos \phi}{\lambda_c}\right) \quad (2.15)$$

$$= a \exp\left(-\frac{j2\pi d}{\lambda_c}\right) \cdot \exp\left(\frac{j2\pi(i-1)\Delta_t \lambda_c \cos \phi}{\lambda_c}\right) \quad (2.16)$$

$$= a \exp\left(-\frac{j2\pi d}{\lambda_c}\right) \cdot \exp(j2\pi(i-1)\Delta_t \cos \phi), \quad i = 1, \dots, n_t. \quad (2.17)$$

The unit spatial signature in the transmit direction of Ω is defined as:

$$\mathbf{e}_t(\Omega) := \frac{1}{\sqrt{n_t}} \begin{bmatrix} 1 \\ \exp(-j2\pi\Delta_t\Omega) \\ \vdots \\ \exp(-j2\pi(n_t-1)\Delta_t\Omega) \end{bmatrix}. \quad (2.18)$$

2.1.3 Antenna arrays with only a line-of-sight (MIMO channel)

Suppose that there are n_t transmit antennas and n_r receive antennas constituting two linear arrays. The channel model is

$$\mathbf{y} = \mathbf{H}\mathbf{x} + \mathbf{w}, \quad (2.19)$$

where \mathbf{y} is the received vector, $\mathbf{H} \in \mathbb{C}^{n_t \times n_r}$ is the channel matrix, \mathbf{x} is the transmitted symbol and $\mathbf{w} \sim \mathcal{CN}(0, N_0 \mathbf{I}_{n_r})$ is the noise [4], [5].

The channel gain between the k^{th} transmit antenna and the i^{th} receive antenna is

$$h_{ik} = a \exp\left(-\frac{j2\pi d_{ik}}{\lambda_c}\right), \quad (2.20)$$

where a is the attenuation of the path (assuming same a for all antennas pairs) and d_{ik} is the distance between the k^{th} transmit antenna and the i^{th} receive antenna.

The distance between the transmitter and the receiver is much larger than size of the antenna arrays and therefore the paths from the transmit antenna to each of the receive antennas are, to a first-order, parallel and

$$d_{ik} \approx d + (i-1)\Delta_r\lambda_c \cos\phi_r - (k-1)\Delta_t\lambda_c \cos\phi_t, \quad (2.21)$$

where d is the distance between the first antenna of transmitter and the first receive antenna, Δ_r is the normalized receive antenna separation, Δ_t is the normalized transmit antenna separation, ϕ_r and ϕ_t are the angles of incidence of the line of sight path on the receive and transmit antenna arrays, respectively and λ_c is the carrier wavelength.

Let us define $\Omega_t := \cos\phi_t$ and $\Omega_r := \cos\phi_r$. Then,

$$h_{ik} = a \exp\left(-\frac{j2\pi d}{\lambda_c}\right) \cdot \exp(-j2\pi(i-1)\Delta_r\Omega_r) \cdot \exp(j2\pi(k-1)\Delta_t\Omega_t), \quad (2.22)$$

and

$$\mathbf{H} = a\sqrt{n_t n_r} \exp\left(-\frac{j2\pi d}{\lambda_c}\right) \mathbf{e}_r(\Omega_r) \mathbf{e}_t^*(\Omega_t). \quad (2.23)$$

All receive spatial signatures are in the same direction as $\mathbf{e}_r(\Omega_r)$ (columns of \mathbf{H}) so there is one spatial degree of freedom available [4].

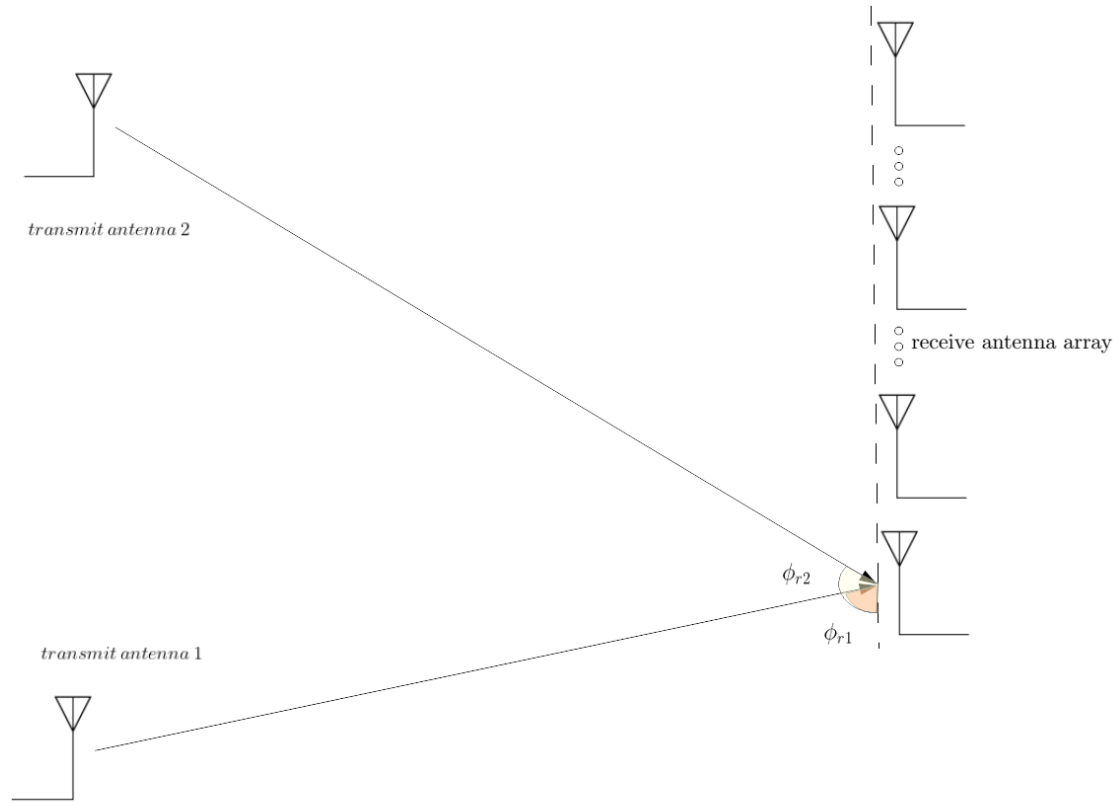


Figure 2.3: Two geographically separated transmit antennas each with line-of-sight to a receive antenna array.

2.1.4 Geographically separated transmit antennas

Without loss of generality, suppose only two transmit antennas, each one with line-of-sight to the receive antenna array. The antenna separation is considered much larger than the distance between the transmitter and the receiver.

The spatial signature of the k^{th} transmit antenna is

$$\mathbf{h}_k = a_k \sqrt{n_r} \exp\left(-\frac{j2\pi d_{1k}}{\lambda_c}\right) \mathbf{e}_r(\Omega_{rk}), \quad k = 1, 2, \quad (2.24)$$

where a_k is the attenuation along the line-of-sight path of the k^{th} transmitter antenna, d_{1k} is the distance between the k^{th} antenna of transmitter and the first receive antenna, $\mathbf{e}_r(\cdot)$ is the unit spatial signature in the directional cosine and $\Omega_{rk} := \cos \phi_{rk}$ (ϕ_{rk} is the angle of incidence) [4]. The channel matrix is given by

$$\mathbf{H} = [\mathbf{h}_1 \ \mathbf{h}_2]. \quad (2.25)$$

The spatial signature $\mathbf{e}_r(\Omega)$ is a periodic function of Ω with period $1/\Delta_r$. So, the columns of \mathbf{H} are linearly independent and not alligned when

$$\Omega_r := \Omega_{r2} - \Omega_{r1} \neq 0 \pmod{\frac{1}{\Delta_r}}. \quad (2.26)$$

Therefore, we have two degrees of freedom and the spatial signatures of the transmit antennas are resolved. On the other hand, the conditioning of \mathbf{H} shows how much alligned are the spatial signatures. The angle θ between the two spatial signatures is given by

$$|\cos \theta| = |\mathbf{e}_r^*(\Omega_{r1})\mathbf{e}_r(\Omega_{r2})|. \quad (2.27)$$

The $\mathbf{e}_r^*(\Omega_{r1})\mathbf{e}_r(\Omega_{r2})$ depends on the difference $\Omega_r := \Omega_{r2} - \Omega_{r1}$. So, we define

$$f_r(\Omega_r) := \mathbf{e}_r^*(\Omega_{r1})\mathbf{e}_r(\Omega_{r2}). \quad (2.28)$$

Hence,

$$f_r(\Omega_r) = \frac{1}{n_r} \exp(-j\pi(n_r - 1)\Delta_r\Omega_r) \frac{\sin(\pi L_r\Omega_r)}{\sin(\pi L_r\Omega_r/n_r)}, \quad (2.29)$$

where $L_r := n_r\Delta_r$ is the normalized length of the receive antenna array. The proof is given in Appendix A.

The $f_r(\Omega_r)$ is periodic with period $n_r/L_r = 1/\Delta_r$. It has a peak at $\Omega_r = 0$, $f_r(0) = 1$ and $f_r(\Omega_r) = 0$ at $k/L_r, k = 1, \dots, n_r - 1$. The main lobe has width $2/L_r$, centered around integer multiples of $1/\Delta_r$.

So, the channel matrix is ill-conditioned (spatial signatures are closer alligned) when

$$\left| \Omega_r - \frac{k}{\Delta_r} \right| \ll \frac{1}{L_r}, k \in \mathbb{Z}. \quad (2.30)$$

Since $\Omega_r \in [-2, 2]$,

$$|\Omega_r| \ll \frac{1}{L_r}, \Delta_r \leq 1/2. \quad (2.31)$$

The parameter $1/L_r$ may be considered as measure of resolvability in the angular domain. If $|\Omega_r| \ll 1/L_r$, then the two transmitted signals can not be resolved by the receive antenna array and there is actually only one degree of freedom. Increasing the number of receive antennas n_r for fixed length L_r of the array, it does not affect the angular resolvability of the receive antenna array which is limited by the $1/L_r$.

The receive beamforming pattern of the vector $\mathbf{e}_r(\cos \phi_0)$ associated with the vector $\mathbf{e}_r(\cos \phi)$ is the polar plot

$$(\phi, f_r(|\cos \phi - \cos \phi_0|)), \quad (2.32)$$

where ϕ_0 is the angle of incidence of a specific path. Optimal detection is achieved by the projection of the receive signal onto the receive beamforming vector $\mathbf{e}_r(\cos \phi_0)$. Signals from any different direction ϕ are attenuated by a factor of

$$|\mathbf{e}_r^*(\cos \phi_0)\mathbf{e}_r(\cos \phi)| = f_r(|\cos \phi - \cos \phi_0|). \quad (2.33)$$

The beamforming pattern has main lobes around ϕ_0 and around any angle ϕ for which

$$\cos \phi = \cos \phi_0 \pmod{\frac{1}{\Delta_r}}, \quad (2.34)$$

and the main lobe has width $2/L_r$ (beam width). It occurs that larger L_r gives narrower beam and higher angular resolution (Figures 2.4 and 2.5) [4].

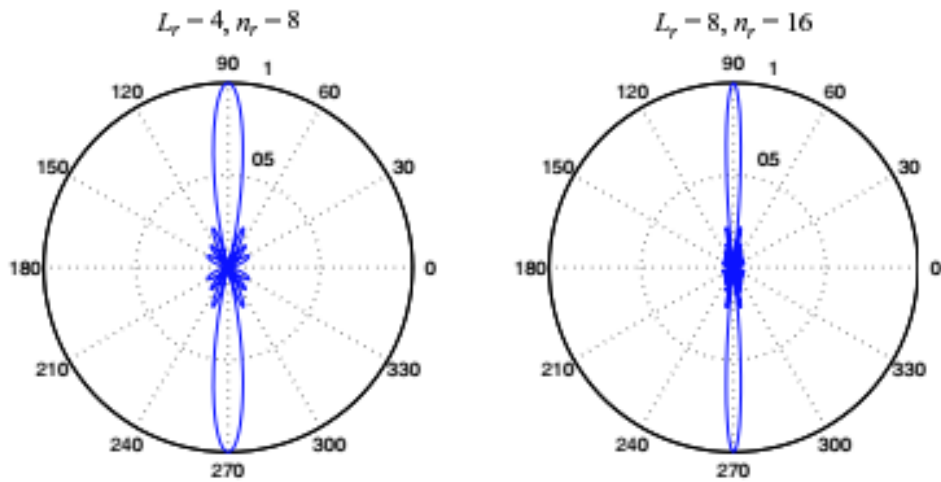


Figure 2.4: Beamforming patterns for different antenna array lengths. (Left) $L_r = 4$ and (right) $L_r = 8$. Antenna separation is fixed at half the carrier wavelength. The larger the length of the array, the narrower the beam ([4]).

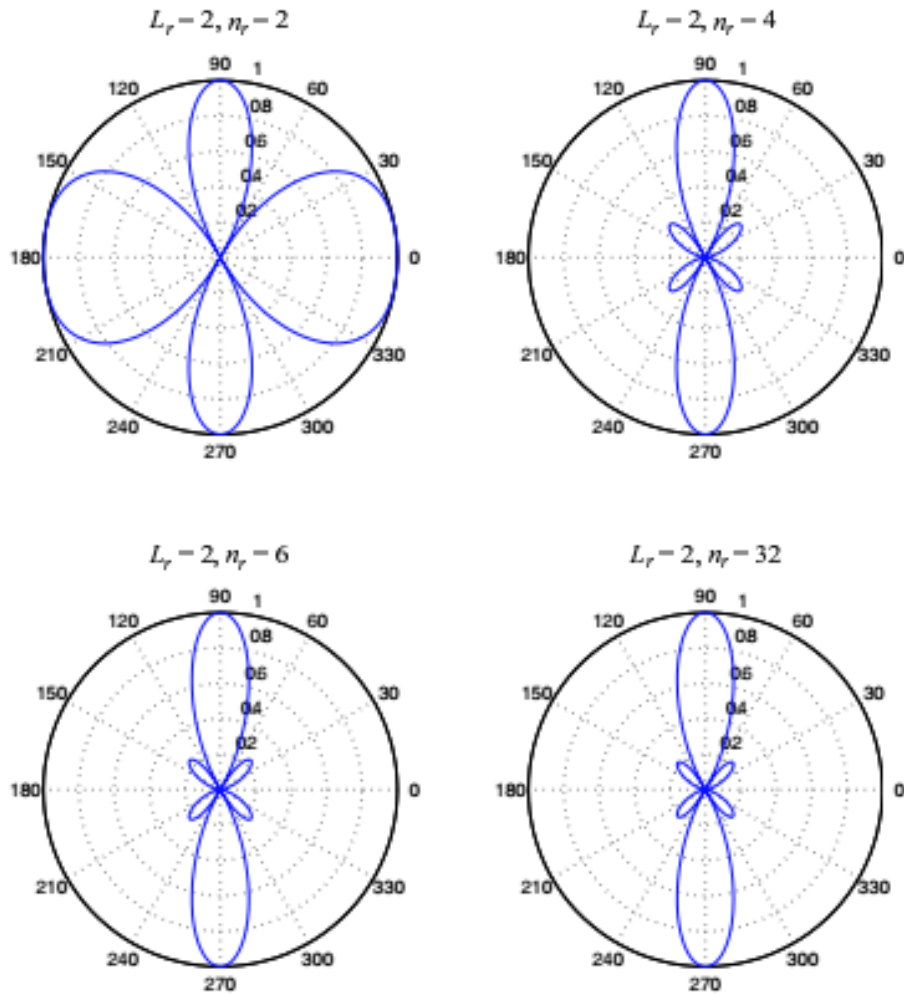


Figure 2.5: Receive beamforming patterns aimed at 90° , with antenna array length $L_r = 2$ and different numbers of receive antennas n_r . Note that the beamforming pattern is always symmetrical about the $0^\circ - 180^\circ$ axis, so lobes always appear in pairs. For $n_r = 4, 6, 32$, the antenna separation $\Delta_r \leq 1/2$, and there is a single main lobe around 90° (together with its mirror image). For $n_r = 2$, $\Delta_r = 1 > 1/2$ and there is an additional pair of main lobes ([4]).

2.1.5 Geographically separated receive antennas

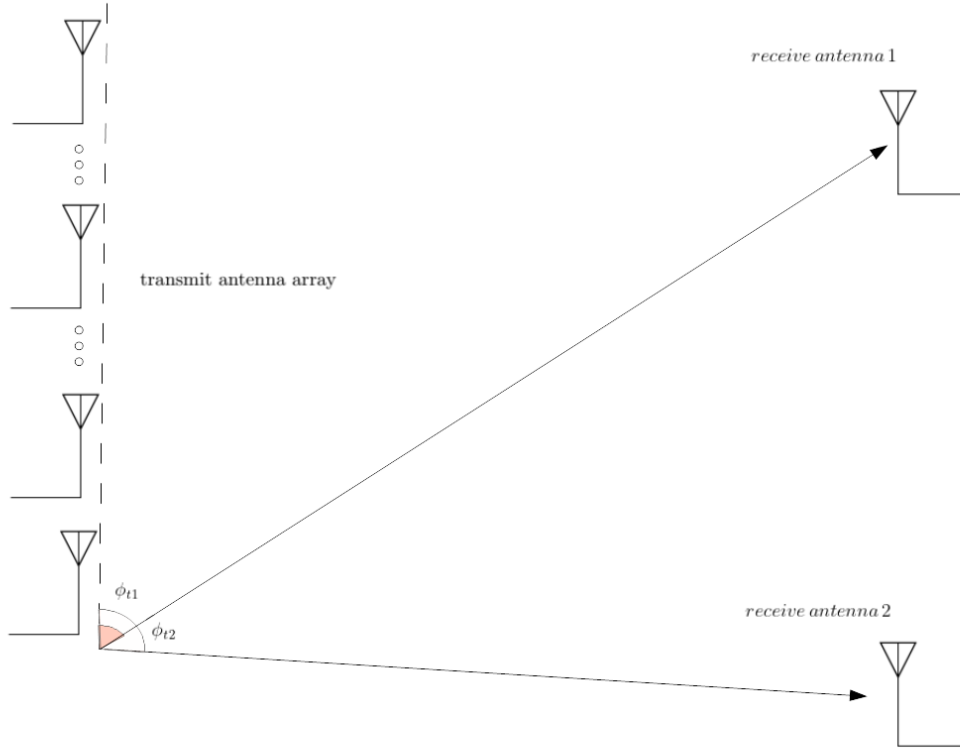


Figure 2.6: Two geographically separated receive antennas each with line of sight from a transmit antenna array.

Suppose the same scenario of geographically separated antennas but on the receiver side.

The channel matrix is

$$\mathbf{H} = [\mathbf{h}_1 \ \mathbf{h}_2]^* \quad (2.35)$$

where

$$\mathbf{h}_i = a_i \sqrt{n_t} \exp\left(\frac{j2\pi d_{i1}}{\lambda_c}\right) \mathbf{e}_t(\Omega_{ti}), \quad i = 1, 2, \quad (2.36)$$

where a_i is the attenuation along the line-of-sight path of the i^{th} receiver antenna, d_{i1} is the distance between the i^{th} antenna of the receiver and the first transmit antenna, $\mathbf{e}_t(\cdot)$ is the unit spatial signature in the directional cosine and $\Omega_i := \cos \phi_{ti}$ (ϕ_{ti} is the angle of incidence) [4].

If it holds that

$$\Omega_t := \Omega_{t2} - \Omega_{t1} \neq 0 \pmod{\frac{1}{\Delta_t}}, \quad (2.37)$$

then the channel matrix \mathbf{H} has two rows that are linearly independent and we could have spatial multiplexing with two degrees of freedom. \mathbf{H} is well-conditioned when the angular separation Ω_t of the two receive antennas is of the same order or larger than $1/L_t$, where $L_t := n_t \Delta_t$ is the normalized length of the transmit antenna array.

The transmit beamforming pattern is similar to the receive beamforming pattern. This represents the transmit power in other directions when the transmitter focuses its signal along a desired direction.

2.1.6 Line-of-Sight MIMO channel with one reflected path

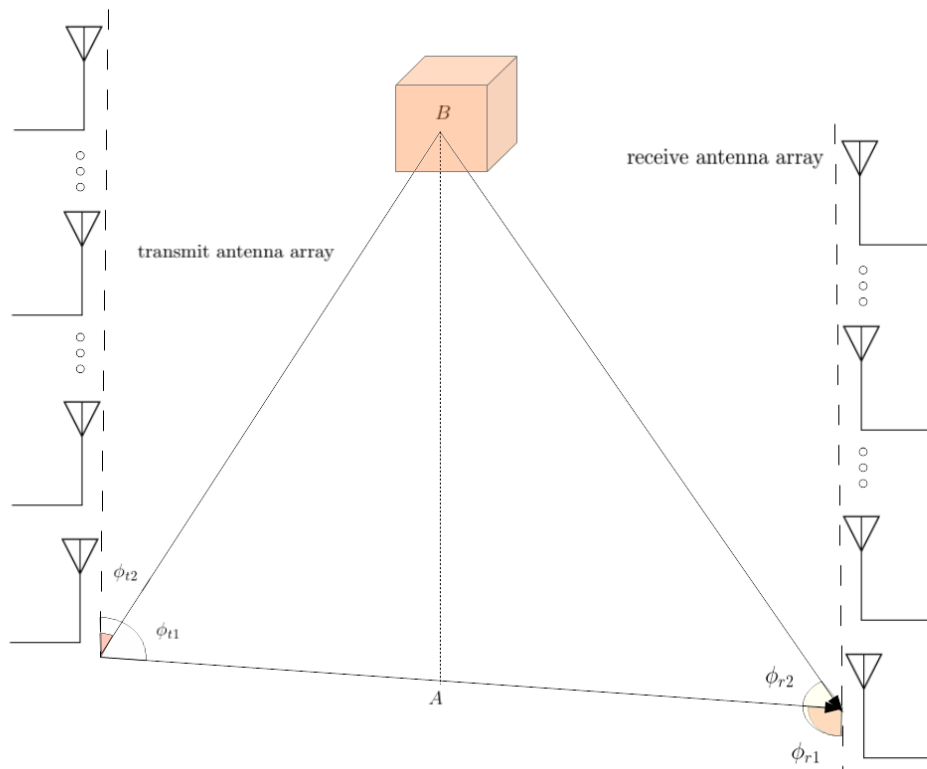


Figure 2.7: MIMO channel with a direct path and a reflected path.

Next, we consider a line-of-sight MIMO channel with one reflected path. In this case, there are antenna arrays at both the transmitter and the receiver side. Except from the line-of-sight path, there is also a path reflected off a wall.

Applying the superposition principle, the channel matrix is

$$\begin{aligned} \mathbf{H} &= a_1 \sqrt{n_t n_r} \exp\left(-\frac{j2\pi d_1}{\lambda_c}\right) \mathbf{e}_r(\Omega_{r1}) \mathbf{e}_t^*(\Omega_{t1}) \\ &+ a_2 \sqrt{n_t n_r} \exp\left(-\frac{j2\pi d_2}{\lambda_c}\right) \mathbf{e}_r(\Omega_{r2}) \mathbf{e}_t^*(\Omega_{t2}) \end{aligned} \quad (2.38)$$

where a_i is the attenuation of the i^{th} path, d_i is the distance between the first antenna of transmitter and the first receive antenna along path i and ϕ_{ri} and ϕ_{ti} are the angles of incidence of the path i on the receive and transmit antenna arrays, respectively ($\Omega_{ri} := \cos \phi_{ri}, \Omega_{ti} := \cos \phi_{ti}$) [4].

The matrix \mathbf{H} is rank 2 if

$$\Omega_{r2} \neq \Omega_{r1} \pmod{\frac{1}{\Delta_r}} \quad (2.39)$$

and

$$\Omega_{t2} \neq \Omega_{t1} \pmod{\frac{1}{\Delta_t}}. \quad (2.40)$$

\mathbf{H} is well-conditioned when the angular separation $|\Omega_t|$ of the two paths at the transmit array is of the same order or larger than $1/L_t$ and the angular separation $|\Omega_r|$ at the receive array is of the same order or larger than $1/L_r$, where

$$\Omega_t = \cos \phi_{t2} - \cos \phi_{t1}, \quad L_t := n_t \Delta_t \quad (2.41)$$

and

$$\Omega_r = \cos \phi_{r2} - \cos \phi_{r1}, \quad L_r := n_r \Delta_r. \quad (2.42)$$

Let us define

$$\mathbf{H}'' = [a_1 \sqrt{n_t n_r} \exp\left(-\frac{j2\pi d_1}{\lambda_c}\right) \mathbf{e}_r(\Omega_{r1}) \quad a_2 \sqrt{n_t n_r} \exp\left(-\frac{j2\pi d_2}{\lambda_c}\right) \mathbf{e}_r(\Omega_{r2})], \quad (2.43)$$

$$\mathbf{H}' = \begin{bmatrix} \mathbf{e}_t^*(\Omega_{t1}) \\ \mathbf{e}_t^*(\Omega_{t2}) \end{bmatrix}. \quad (2.44)$$

Then, channel \mathbf{H} is the product of geographically separated transmit antennas channel \mathbf{H}' and geographically separated receive antennas channel \mathbf{H}''

$$\mathbf{H} = \mathbf{H}'' \mathbf{H}'. \quad (2.45)$$

If the parameter $\Omega_r L_r \ll 1$ or the parameter $\Omega_t L_t \ll 1$ specifically, one of two channels \mathbf{H}' and \mathbf{H}'' is ill-conditioned, then the overall channel matrix is also ill-conditioned. The MIMO channel with a direct path and a reflected path can be interpreted as a concatenation of the n_t by 2 geographically separated receive antennas channel and the 2 by n_r geographically separated transmit antennas channel. Particularly, there are two virtual “relays” one at the point A and one at the point B, which are geographically separated and make it possible to have two degrees of freedom, although both the transmit antennas and the receive antennas are close together (Figures 2.7 and 2.8) [4].

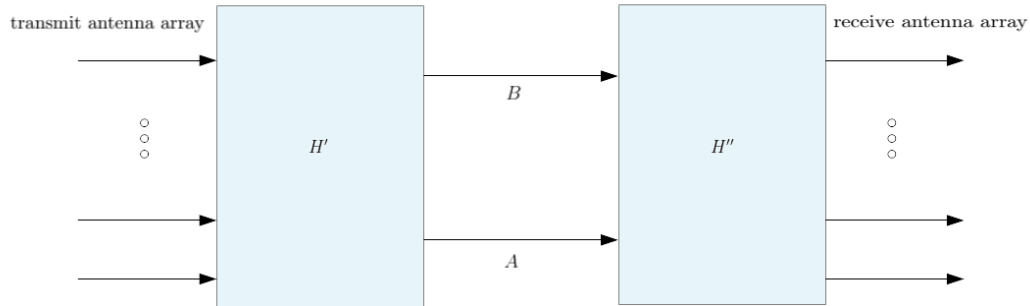


Figure 2.8: Channel is viewed as a concatenation of two channels \mathbf{H}' and \mathbf{H}'' with intermediate (virtual) relays A and B.

2.2 Modeling of MIMO Fading Channels

2.2.1 Basic Approach

Physical models of the MIMO channel in terms of individual multipaths do not offer a level of abstraction from design perspective. So, one approach is to abstract the physical model into a higher-level model in terms of spatially resolvable paths [4].

The transmit and receive antenna array lengths, L_t and L_r , define the degree of resolvability in the angular domain. In particular, paths whose transmit directional cosines differ by less than $1/L_t$ and receive directional cosines differ by less than $1/L_r$ are not resolvable. Hence, the angular domain is divided at fixed angular spacings of $1/L_t$ at the transmitter and at fixed angular spacings of $1/L_r$ at the receiver, and represent the channel in terms of these new input and output coordinates. The $(k, l)^{th}$ channel gain in these angular coordinates is the aggregation of all paths whose transmit directional cosine is within an angular window of width $1/L_t$ around l/L_t and whose receive directional cosine is within an angular window of width $1/L_r$ around k/L_r .

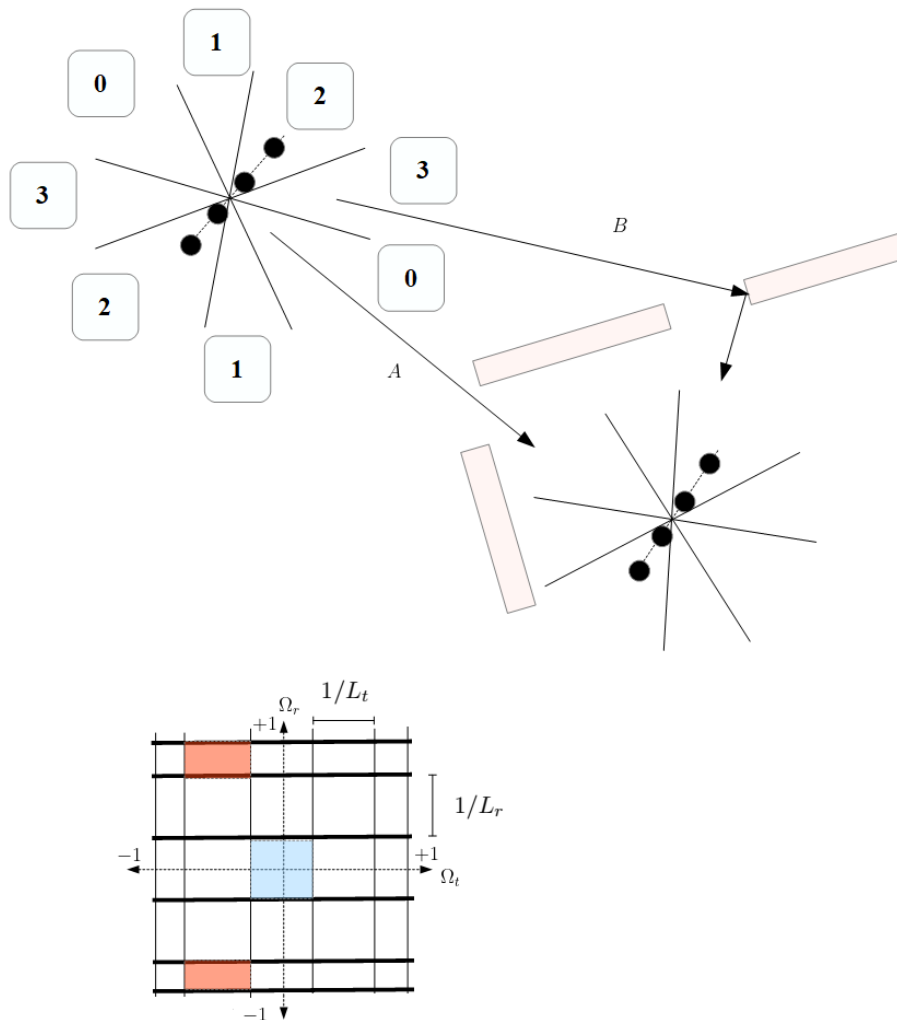


Figure 2.9: An illustration of the MIMO channel in the angular domain and the resolvable bins. There are a transmitter with 4 antennas ($L_t = 2$) and a receiver with 4 antennas ($L_r = 2$). Moreover, the receiver is inside a building. Also, there are a line-of-sight path (path *A*) and a reflected path (path *B*). Due to the limited resolvability of the antenna arrays, the physical paths are partitioned into resolvable bins of angular widths $1/L_r$ by $1/L_t$.

2.2.2 MIMO Multipath Channel

Consider the narrowband MIMO channel [4]

$$\mathbf{y} = \mathbf{H}\mathbf{x} + \mathbf{w}. \quad (2.46)$$

If we have an arbitrary number of physical paths between the transmitter and the receiver, then the channel matrix \mathbf{H} is given by

$$\mathbf{H} = \sum_i a_i^b \mathbf{e}_r(\Omega_{ri}) \mathbf{e}_t^*(\Omega_{ti}), \quad (2.47)$$

where

$$a_i^b = a_i \sqrt{n_t n_r} \exp\left(-\frac{j2\pi d^{(i)}}{\lambda_c}\right). \quad (2.48)$$

Path i has an attenuation of a_i , $d^{(i)}$ is the distance between transmit antenna 1 and receive antenna 1 along path i and ϕ_{ri} and ϕ_{ti} are the angles of incidence of the path i on the receive and transmit antenna arrays, respectively ($\Omega_{ri} := \cos \phi_{ri}$, $\Omega_{ti} := \cos \phi_{ti}$).

2.2.3 Angular Domain Representation of Signals

The received signal has the unit spatial signature $\mathbf{e}_r(\Omega)$ in the directional cosine Ω . Consider,

$$f_r(\Omega) := \mathbf{e}_r^*(0) \mathbf{e}_r(\Omega) = \frac{1}{n_r} \exp(-j\pi(n_r - 1)\Delta_r \Omega) \frac{\sin(\pi L_r \Omega)}{\sin(\pi L_r \Omega / n_r)}. \quad (2.49)$$

Also, for $k = 1, \dots, n_r - 1$, we have

$$f_r(0) = 1, f_r\left(\frac{k}{L_r}\right) = 0, f_r\left(\frac{-k}{L_r}\right) = f_r\left(\frac{n_r - k}{L_r}\right). \quad (2.50)$$

So, the fixed n_r vectors

$$\mathcal{S}_r = \left\{ \mathbf{e}_r(0), \mathbf{e}_r\left(\frac{1}{L_r}\right), \dots, \mathbf{e}_r\left(\frac{n_r - 1}{L_r}\right) \right\} \quad (2.51)$$

form an orthonormal basis for the received signal space \mathbb{C}^{n_r} . This basis provides the representation of the received signals in the angular domain.

From the beamforming patterns of the angular basis vectors, we notice that each basis vector has at least one pair of main lobes of width $2/L_r$ and small side lobes. The different basis vectors $\mathbf{e}_r(k/L_r)$'s have different main lobes. So, the received signal along any physical direction will have most of its energy along one particular $\mathbf{e}_r(k/L_r)$ vector and very little along all the others. Therefore, this orthonormal basis provides a simple

but approximate decomposition of the total received signal into the multipaths received along the different physical directions with a resolution of $1/L_r$.

Similarly, for the transmitted signal, we have that the fixed n_t vectors

$$\mathcal{S}_t = \left\{ \mathbf{e}_t(0), \mathbf{e}_t\left(\frac{1}{L_t}\right), \dots, \mathbf{e}_t\left(\frac{n_t-1}{L_t}\right) \right\} \quad (2.52)$$

form an orthonormal basis for the transmitted signal space \mathbb{C}^{n_t} . This basis provides the representation of the transmitted signals in the angular domain [4].

Examples of Angular Bases

There are three cases (Figure 2.10) [4]:

1. Antennas are critically spaced at half the wavelength ($\Delta_r = 1/2$). Each of the basis vectors $\mathbf{e}_r(k/L_r)$ has a single pair of main lobes around the angles $\pm \cos^{-1}(k/L_r)$.
2. Antennas are sparsely spaced ($\Delta_r > 1/2$). In this case, some of the basis vectors have more than one pair of main lobes.
3. Antennas are densely spaced ($\Delta_r < 1/2$). Some of the basis vectors have no main lobes.

There is a one-to-one correspondence between the angular windows and the angular basis vectors, in the critically-spaced antennas.

Angular Domain Transformation as DFT

Let \mathbf{U}_t be the $n_t \times n_t$ unitary matrix the columns of which are the basis vectors in \mathcal{S}_t . If \mathbf{x} and \mathbf{x}^a are the n_t -dimensional vector of transmitted signals from the antenna array and its angular domain representation respectively, then

$$\mathbf{x} = \mathbf{U}_t \mathbf{x}^a, \quad \mathbf{x}^a = \mathbf{U}_t^* \mathbf{x}. \quad (2.53)$$

The $(k, l)^{th}$ entry of \mathbf{U}_t is

$$\frac{1}{\sqrt{n_t}} \exp\left(-\frac{j2\pi kl}{n_t}\right) \quad k, l = 0, \dots, n_t - 1. \quad (2.54)$$

So, the angular domain representation \mathbf{x}^a is the Inverse Discrete Fourier Transform of \mathbf{x} [4].

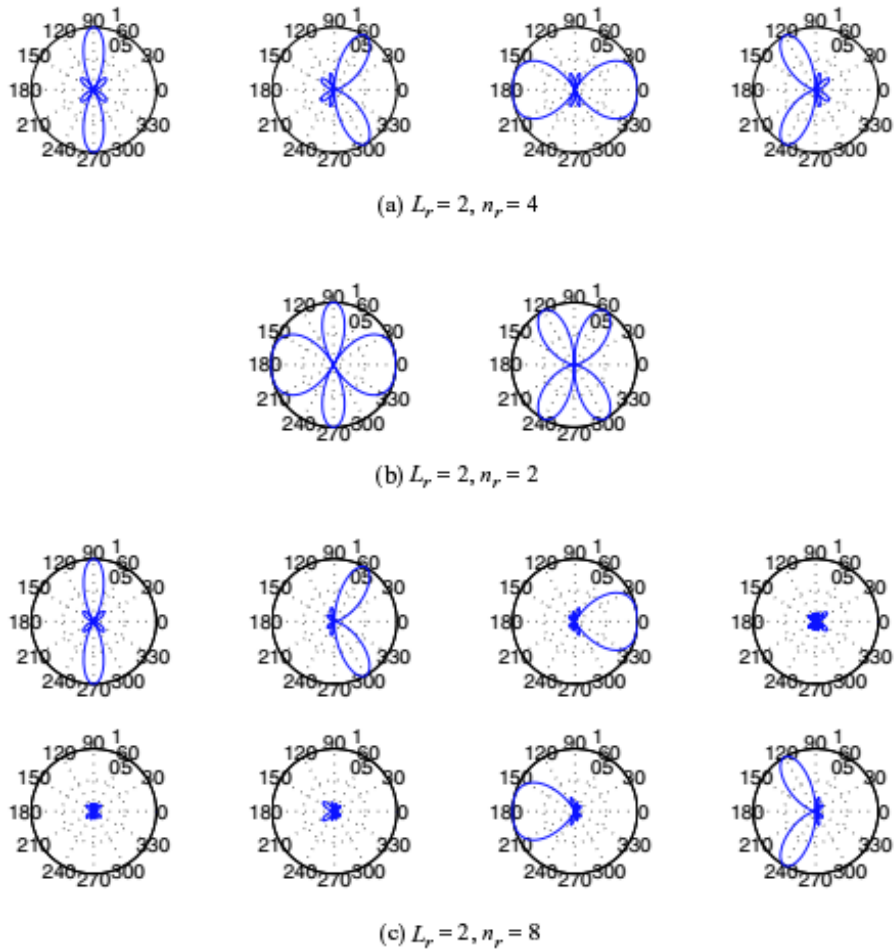


Figure 2.10: Receive beamforming patterns of the angular basis vectors. Independent of the antenna spacing, the beamforming patterns all have the same beam widths for the main lobe, but the number of main lobes depends on the spacing. (a) Critically-spaced case (b) Sparsely-spaced case (c) Densely-spaced case([4]).

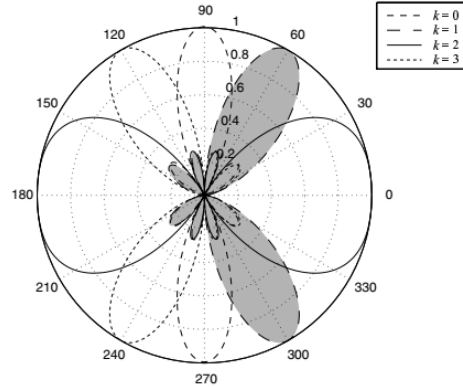


Figure 2.11: The bin \mathcal{R}_k is the set of all paths that arrive roughly in the direction of the main lobes of the beamforming pattern of $\mathbf{e}_r(k/L)$. Here $L_r = 2$ and $n_r = 4$ ([4]).

2.2.4 Angular Domain Representation of MIMO Channels

We recall that \mathbf{U}_t is the $n_t \times n_t$ unitary matrix the columns of which are the basis vectors in \mathcal{S}_t and \mathbf{U}_r is the $n_r \times n_r$ unitary matrix the columns of which are the basis vectors in \mathcal{S}_r (DFT matrices). The angular domain representation of the transmitted and received signals is given by

$$\mathbf{x}^a = \mathbf{U}_t^* \mathbf{x}, \quad (2.55)$$

$$\mathbf{y}^a = \mathbf{U}_r^* \mathbf{y}. \quad (2.56)$$

So, the equivalent representation of the channel in the angular domain is

$$\mathbf{y}^a = \mathbf{U}_r^* \mathbf{H} \mathbf{U}_t \mathbf{x}^a + \mathbf{U}_r^* \mathbf{w} \quad (2.57)$$

$$\mathbf{y}^a = \mathbf{H}^a \mathbf{x}^a + \mathbf{w}^a, \quad (2.58)$$

where

$$\mathbf{H}^a := \mathbf{U}_r^* \mathbf{H} \mathbf{U}_t \quad (2.59)$$

and

$$\mathbf{w}^a := \mathbf{U}_r^* \mathbf{w} \sim \mathcal{CN}(0, N_0 \mathbf{I}_{n_r}). \quad (2.60)$$

The $(k, l)^{th}$ entry of the channel matrix \mathbf{H}^a is

$$h_{kl}^a = \mathbf{e}_r^*(k/L_r) \mathbf{H} \mathbf{e}_t(l/L_t) \quad (2.61)$$

$$= \sum_i a_i^b [\mathbf{e}_r^*(k/L_r) \mathbf{e}_r(\Omega_{ri})] \cdot [\mathbf{e}_t^*(\Omega_{ti}) \mathbf{e}_t(l/L_t)]. \quad (2.62)$$

Let \mathcal{R}_k be the set of physical paths whose receive directional cosine is within a window of width $1/L_r$ around k/L_r (Figure 2.11) and \mathcal{T}_l be the set of physical paths whose transmit directional cosine is within a window of width $1/L_t$ around l/L_t . The element h_{kl}^a is the aggregation of the gains a_i^b of the physical paths in $\mathcal{T}_l \cap \mathcal{R}_k$, in particular, is the channel gain of angular bin (k, l) . Last, the physical paths that belong to $\mathcal{T}_l \cap \mathcal{R}_k$ are unresolvable in the angular domain [4].

2.2.5 Statistical Modeling in the Angular Domain

The basis for the statistical modeling of the MIMO fading channel is the approximation that the physical paths are partitioned into angularly resolvable bins and aggregated to form resolvable paths whose gains are $h_{kl}^a[m]$. Assuming that the gains $a_i^b[m]$ of the physical paths are independent, we can model the resolvable path gains $h_{kl}^a[m]$ as independent. Moreover, the angles $\{\phi_{ri}[m]\}_m$ and $\{\phi_{ti}[m]\}_m$ typically evolve at a much slower time-scale than the gains $\{a_i^b[m]\}_m$. Therefore, within the time-scale of interest, it is reasonable to assume that paths do not move from one angular bin to another, and the processes $\{h_{kl}^a[m]\}_m$ can be modelled as independent across k and l . In an angular bin (k, l) , where there are many physical paths, applying the Central Limit Theorem, gain $h_{kl}^a[m]$ is modeled as complex circular symmetric Gaussian process and if the angular bin contains no paths, the entries $h_{kl}^a[m]$ can be considered as 0. For a channel with limited angular spread at the receive or the transmit side, many entries of $\mathbf{H}^a[m]$ may be zero (Figures 2.12 and 2.13) [4].

2.3 Sparsity structures in Massive MIMO channel

2.3.1 Massive MIMO

Massive MIMO scales up conventional MIMO by having antenna arrays with a few hundred antennas simultaneously serving many tens of terminals in the same time-frequency resource [1]. Some benefits of Massive MIMO are that it offers improved energy and spectral efficiency. Also, it can achieve higher capacity for cellular systems. In order to exploit these benefits, good channel knowledge is required at both the uplink and the downlink. Acquiring high-dimensional channel side information (CSI) is a challenging problem in massive MIMO. In frequency-division duplexing (FDD) mode, training overhead is proportional to the dimension of Base Station (BS) antenna. In time-division duplexing (TDD) massive MIMO systems, channel reciprocity could be exploited but the training overhead is proportional to the number of active user equipments (UEs) which, if it increases, it could cause pilot contamination by the reuse of the same uplink pilots [2],[3].

2.3. SPARSITY STRUCTURES IN MASSIVE MIMO CHANNEL

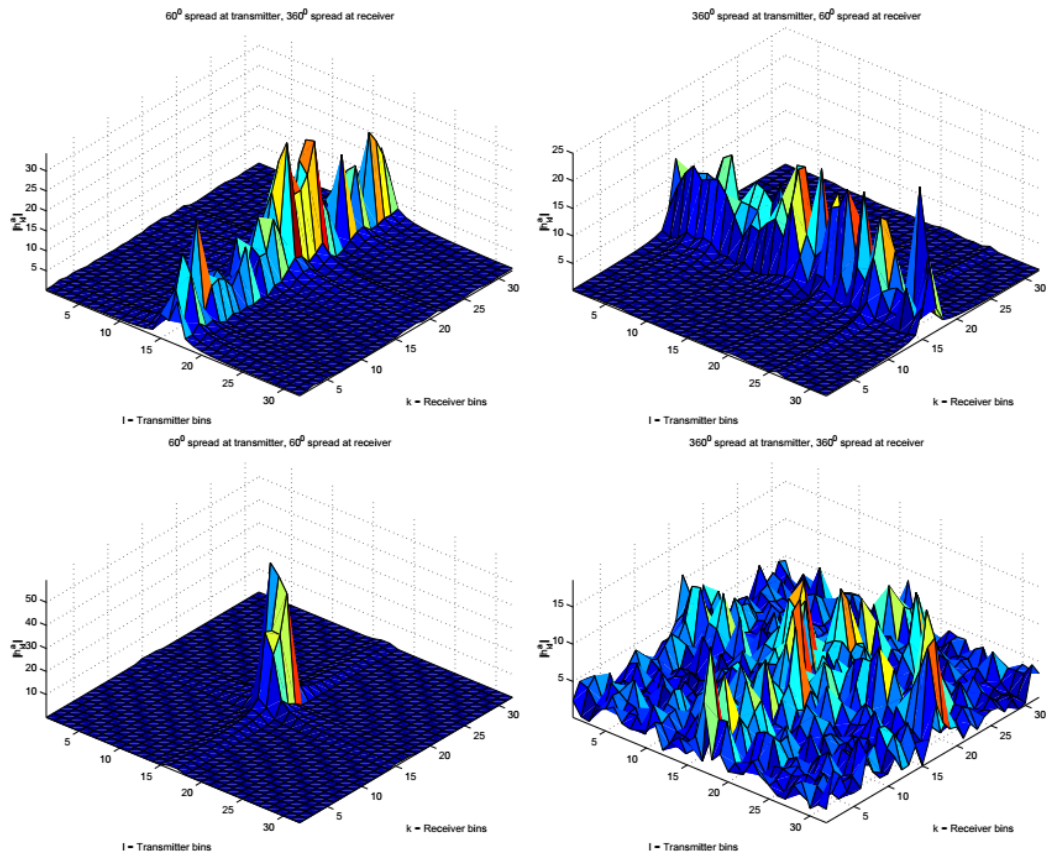


Figure 2.12: Some examples of \mathbf{H}^a . (a) Small angular spread at the transmitter. (b) Small angular spread at the receiver. (c) Small angular spreads at both the transmitter and the receiver. (d) Full angular spreads at both the transmitter and the receiver ([4]).

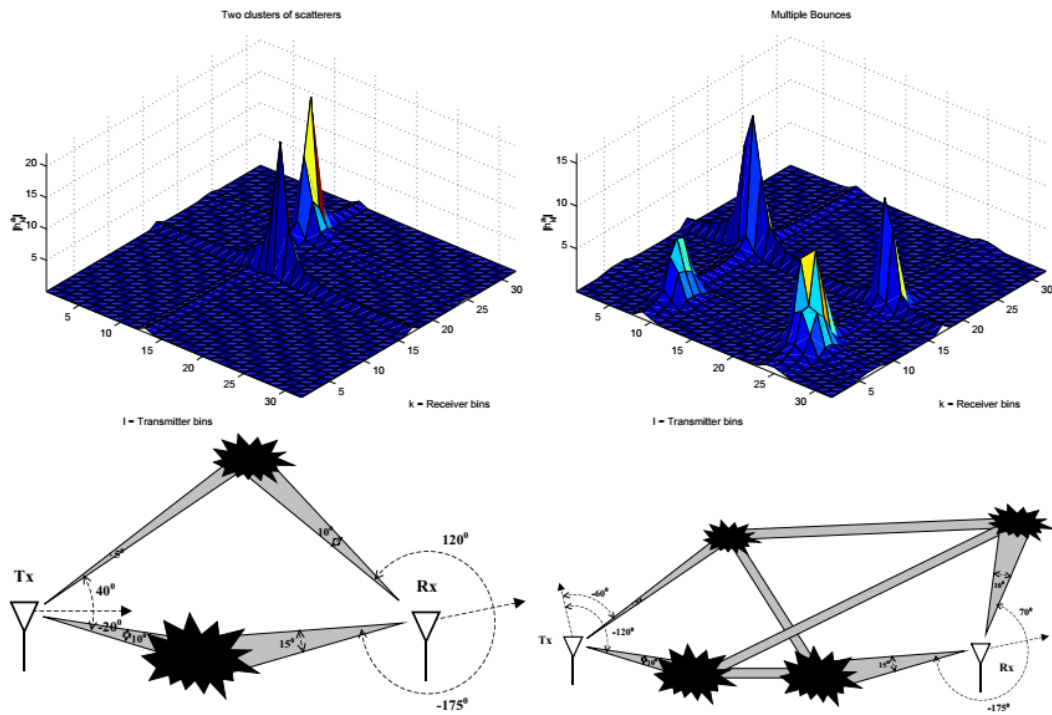


Figure 2.13: Some examples of \mathbf{H}^a . (a) Two clusters of scatterers, with all paths going through a single bounce. (b) Paths scattered via multiple bounces ([4]).

2.3.2 Sparsity structures

In [4], it is stated that if the channel has limited angular spread at the transmitter or the receiver, then the channel matrix \mathbf{H}^a has many zeros. In experimental studies ([7], [8]), it has been observed that Massive MIMO channels are highly correlated at the transmitter side, however, the receive correlation is lower. This happens because there is rich local scattering at the receiver. BS is usually elevated higher than local scatterers and far away from UE, therefore, it occurs limited angular spread. Also, the channel matrix via angular domain representation is sparse [9].

Chapter 3

Problem statement

We consider a massive MIMO system operating in FDD mode. There is one BS and K single-antenna UEs. The BS has an ULA with M antenna elements. Let us assume that M is much larger than the number of served UEs and channels between BS and UEs are flat block-fading. During the downlink training, the received signal vector at an UE is

$$\mathbf{y} = \mathbf{A}\mathbf{h} + \mathbf{w}, \quad (3.1)$$

where $\mathbf{A} \in \mathbb{C}^{N \times M}$ is the training matrix, $\mathbf{h} \in \mathbb{C}^{M \times 1}$ is the channel vector and $\mathbf{w} \in \mathbb{C}^{N \times 1}$ is the additive noise [5].

In FDD mode, the amount of training overhead is proportional to the dimension of BS antenna array. The required training overhead N for conventional least squares (LS) and minimum mean square error (MMSE) estimators scales linearly with the number of BS antennas [2], [5]. It is obvious that CSI acquisition at BS is a challenging task because, as M increases for massive MIMO, the training overhead becomes prohibitively large.

On the other hand, there are sparsity-inspired approaches that they provide overhead reduction based on the sparsity of the channel representation in the angular domain $\mathbf{h}^{\mathbf{a}}$ [3], [6].

In this section, we present the weighted ℓ_1 minimization method using partial support information and our proposal, which achieve low-overhead training [3].

3.1 Partial Support Information

Partial support information is the estimated support \hat{T} of the channel $\mathbf{h}^{\mathbf{a}}$ (Figure 3.1), occurring from the resolvable paths of the limited angles of departure (AoDs). \hat{T} is the set which includes the indices of the elements of the $\mathbf{h}^{\mathbf{a}}$ that are predicted to be non zero and $\text{card}(\hat{T}) = \hat{s}$. The estimated support could be found by the estimation of the AoDs or knowing the mean AoD and the Angular Spread deviation. The accuracy of the estimation is given by the parameter a with $a \in [0, 1]$. For instance, if $a = 0.8$ and $\hat{s} = 20$ then

$$\text{card}(T \cap \hat{T}) = \lfloor a\hat{s} \rfloor = 16.$$



Figure 3.1: Illustration of partial support information ($T = \{3, 4, 5, 7\}$, $\hat{T} = \{3, 4, 5, 8\}$ and $\text{card}(T \cap \hat{T}) = \lfloor a\hat{s} \rfloor = \lfloor \frac{3}{4} \cdot 4 \rfloor = 3$).

3.2 Weighted ℓ_1 minimization using Partial Support Information

Given a vector of channel measurements

$$\mathbf{y} = \mathbf{A}\mathbf{U}\mathbf{h}^{\mathbf{a}} + \mathbf{e} \quad (3.2)$$

the channel recovery problem is formulated as follows [3]:

$$\begin{aligned} \min_{\hat{\mathbf{h}}^{\mathbf{a}} \in \mathbb{C}^M} \quad & \left\| \hat{\mathbf{h}}^{\mathbf{a}} \right\|_{1, \mathbf{w}} \\ \text{subject to} \quad & \left\| \mathbf{A}\mathbf{U}\hat{\mathbf{h}}^{\mathbf{a}} - \mathbf{y} \right\|_2 \leq \epsilon, \\ \text{with} \quad & w_i = \begin{cases} 1, & w_i \notin \hat{T}, \\ 0, & w_i \in \hat{T}, \end{cases} \end{aligned} \quad (3.3)$$

where $\mathbf{A} \in \mathbb{C}^{N \times M}$ is a known Gaussian random matrix of independent complex normal entries with distribution $\mathcal{CN}(0, 1/N)$, \mathbf{e} is the noise ($\|\mathbf{e}\|_2 \leq \epsilon$) and

$$\left\| \hat{\mathbf{h}}^{\mathbf{a}} \right\|_{1, \mathbf{w}} = \sum_{i=1}^{i=M} w_i |\hat{h}_i^{\mathbf{a}}|.$$

In this formulation, the entries that are expected to be zero are weighed more heavily than others in the objective function. \hat{T} is the partial support information of $\mathbf{h}^{\mathbf{a}}$, where $\hat{T} \subseteq \{1, \dots, M\}$ and $\text{card}(\hat{T}) = \hat{s}$. We assume that \hat{T} is available at the UE.

3.3 Weighted ℓ_1 minimization method with different weights

We extend the approach of [3], by selecting weights that are not the conventional zeros and ones. Also, we examine the performance of the proposed method with respect to the accuracy of prior information that is described by the parameter a .

Hence, channel recovery problem becomes:

$$\begin{aligned}
 & \min_{\hat{\mathbf{h}}^{\mathbf{a}} \in \mathbb{C}^M} \quad \left\| \hat{\mathbf{h}}^{\mathbf{a}} \right\|_{1, \mathbf{w}} \\
 & \text{subject to} \quad \left\| \mathbf{A} \mathbf{U} \hat{\mathbf{h}}^{\mathbf{a}} - \mathbf{y} \right\|_2 \leq \epsilon, \\
 & \text{with} \quad w_i = \begin{cases} w_a, & w_i \notin \hat{T}, \\ w_b, & w_i \in \hat{T}. \end{cases}
 \end{aligned} \tag{3.4}$$

This formulation is distinct by the fact that the elements of $\hat{\mathbf{h}}^{\mathbf{a}}$ which we believe that are zero are penalized more than those that belong to the estimated support by the choice of w_a and w_b , respectively. Here, $0.5 \leq w_a \leq 1$ and $0 \leq w_b \leq 0.5$. We study three settings for (w_b, w_a) , specifically, $(0.2, 0.8)$, $(0.4, 0.9)$ and $(0.5, 1)$.

Chapter 4

Numerical results

In this section, we conduct experiments in order to estimate the performance of the proposed weighted ℓ_1 minimization method utilizing partial support information. The non zero elements of channel vector $\hat{\mathbf{h}}^{\mathbf{a}}$ are i.i.d. complex normal with distribution $\mathcal{CN}(0,1)$. Also, we assume that the additive noise vector \mathbf{e} has elements which are i.i.d complex normal random variables. In order to generate the experimental data, we perform 200 Monte Carlo simulations for each figure. We used CVX to solve the minimization problems [10].

4.1 Quality of the estimated CSI versus the training overhead

In Figures 4.1–4.4, we examine how the accuracy of the partial support information, which is described by the parameter a , affects the quality of CSI estimation. As a performance metric, we use the normalized mean square error (NMSE) which is $\mathbb{E} \left[\frac{\|\hat{\mathbf{h}}^{\mathbf{a}} - \mathbf{h}^{\mathbf{a}}\|_2^2}{\|\mathbf{h}^{\mathbf{a}}\|_2^2} \right]$, where $\mathbf{h}^{\mathbf{a}}$ is the channel vector and $\hat{\mathbf{h}}^{\mathbf{a}}$ is the estimated channel. The noise \mathbf{e} is complex standard Gaussian random vector, but we normalize its ℓ_2 norm. Also, we compare three empirical NMSE curves, having different values of a , with simple ℓ_1 minimization without any prior information and Genie-aided LS as a baseline. In Genie-aided LS, we assume that UE has accurate knowledge of channel support and the channel is estimated by LS utilizing that information.

It is obvious that, as the number of measurements becomes larger, the NMSE decreases. We noticed that if the parameter a increases, then NMSE becomes lower. So, higher quality of the partial support information provides better channel recovery. On the other hand, poor accuracy of prior information (i.e. Fig. 4.1 and 4.2 $a = 0.6$) gives worse NMSE than not using any information about the channel support.

4.1. QUALITY OF THE ESTIMATED CSI VERSUS THE TRAINING OVERHEAD

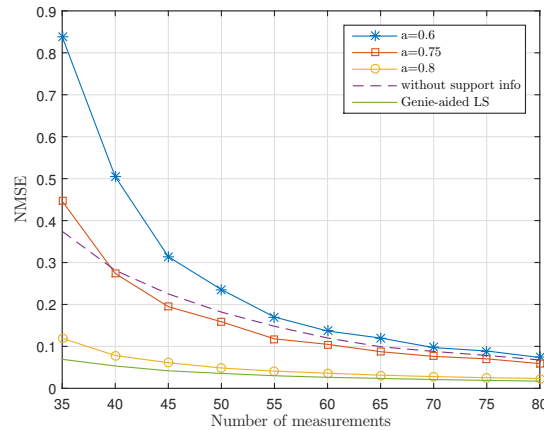


Figure 4.1: Normalized mean square error versus number of measurements with $M = 100$, $s = 20$, $\hat{s} = 25$ and $\|\mathbf{e}\|_2 = 1$.

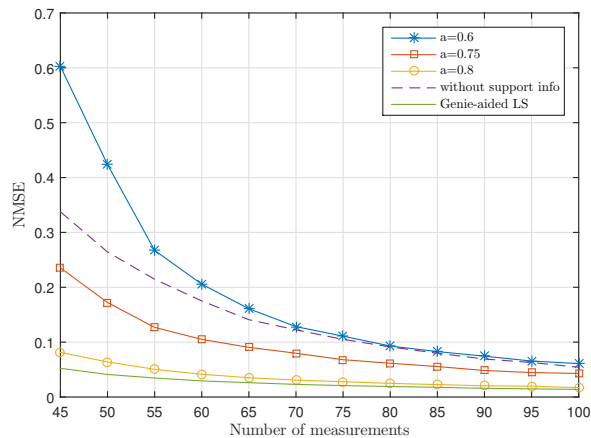


Figure 4.2: Normalized mean square error versus number of measurements with $M = 128$, $s = 25$, $\hat{s} = 32$ and $\|\mathbf{e}\|_2 = 1$.

In Figure 4.5, we compare the curves which occur by having different values of the cardinality \hat{s} of the estimated support. High accuracy defined by the parameter a provides better performance than without any prior knowledge utilization and, in that occasion, partial support information should be exploited. Moreover, in these conditions, if \hat{s} is high enough, then performance is similar with Genie-aided LS.

In Figure 4.6, if the quality of prior knowledge is poor, it would not offer any advantage against standard ℓ_1 minimization method. Hence, we should use accurate estimation of the channel support in order to achieve better performance.

4.1. QUALITY OF THE ESTIMATED CSI VERSUS THE TRAINING OVERHEAD

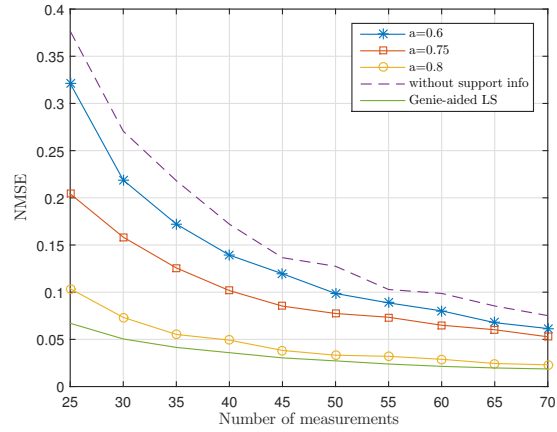


Figure 4.3: Normalized mean square error versus number of measurements with $M = 128, s = 8, \hat{s} = 10$ and $\|\mathbf{e}\|_2 = 1$.

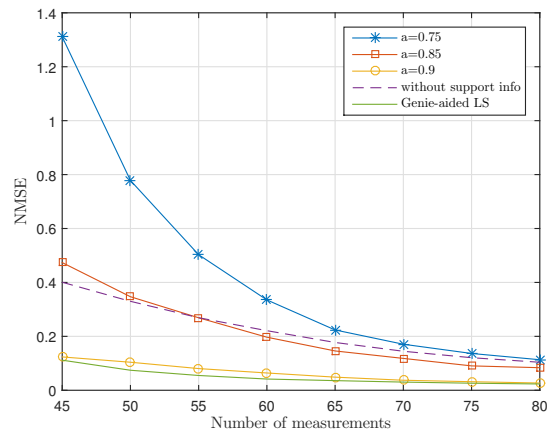


Figure 4.4: Normalized mean square error versus number of measurements with $M = 100, s = 36, \hat{s} = 40$ and $\|\mathbf{e}\|_2 = 1$.

4.1. QUALITY OF THE ESTIMATED CSI VERSUS THE TRAINING OVERHEAD

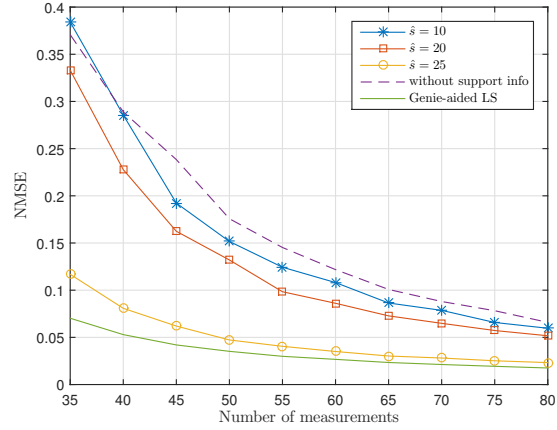


Figure 4.5: NMSE versus number of measurements with $M = 100$, $s = 20$, $a = 0.8$ and $\|\mathbf{e}\|_2 = 1$.

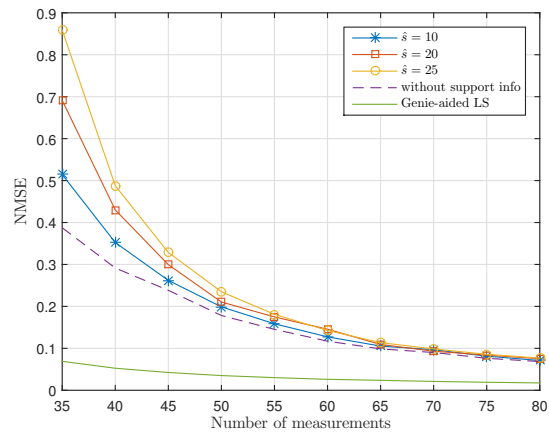


Figure 4.6: NMSE versus number of measurements with $M = 100$, $s = 20$, $a = 0.6$ and $\|\mathbf{e}\|_2 = 1$.

4.2. COMPARISON OF SIMPLE WEIGHTED ℓ_1 MINIMIZATION METHOD TO METHODS WITH DIFFERENT WEIGHTS

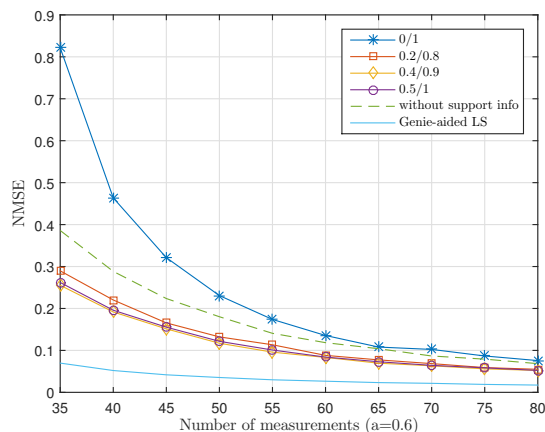


Figure 4.7: NMSE versus number of measurements with $M = 100$, $s = 20$, $\hat{s} = 25$, $a = 0.6$ and $\|\mathbf{e}\|_2 = 1$.

4.2 Comparison of simple weighted ℓ_1 minimization method to methods with different weights

In Figures 4.7–4.13, we compare the weighted ℓ_1 minimization with similar methods which do not have the standard weights zero and one (0/1). In particular, we propose three different methods with weights for the zero entries of $\hat{\mathbf{h}}^a$ 0.8, 0.9, and 1, and for the non zero entries 0.2, 0.4, 0.5, respectively. In the same figures, there are standard ℓ_1 minimization without any prior information and Genie-aided LS.

We noticed that different weights methods outperform the standard weighted ℓ_1 minimization when the quality of the estimated prior information is not high (i.e. Fig. 4.7 and 4.10 $a = 0.6$). Also, the method with weights 0.4/0.9 is slightly better than the two other methods. Lastly, if we have a very good accuracy (i.e. Fig. 4.9 and 4.13) then it is preferred to use the standard weighted ℓ_1 minimization because it has not any significant drawback against the others.

4.2. COMPARISON OF SIMPLE WEIGHTED ℓ_1 MINIMIZATION METHOD TO METHODS WITH DIFFERENT WEIGHTS

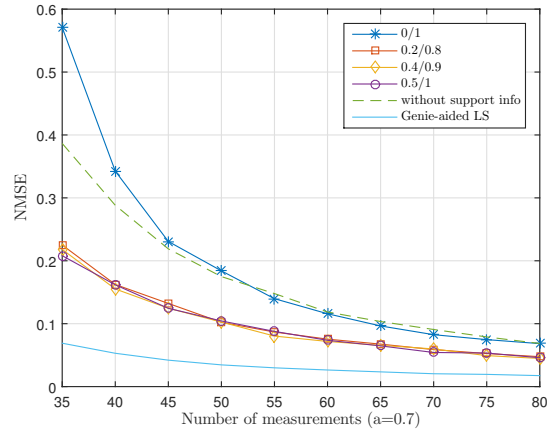


Figure 4.8: NMSE versus number of measurements with $M = 100$, $s = 20$, $\hat{s} = 25$, $a = 0.7$ and $\|\mathbf{e}\|_2 = 1$.

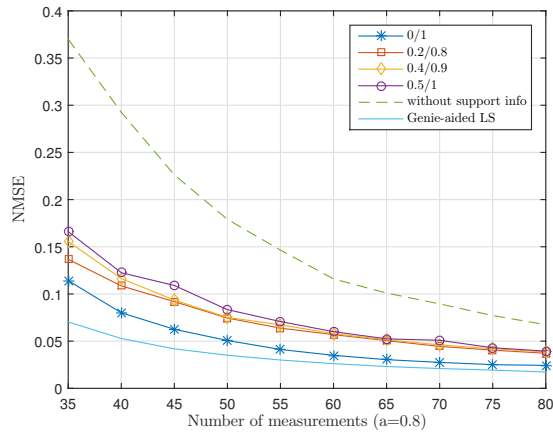


Figure 4.9: NMSE versus number of measurements with $M = 100$, $s = 20$, $\hat{s} = 25$, $a = 0.8$ and $\|\mathbf{e}\|_2 = 1$.

4.2. COMPARISON OF SIMPLE WEIGHTED ℓ_1 MINIMIZATION METHOD TO METHODS WITH DIFFERENT WEIGHTS

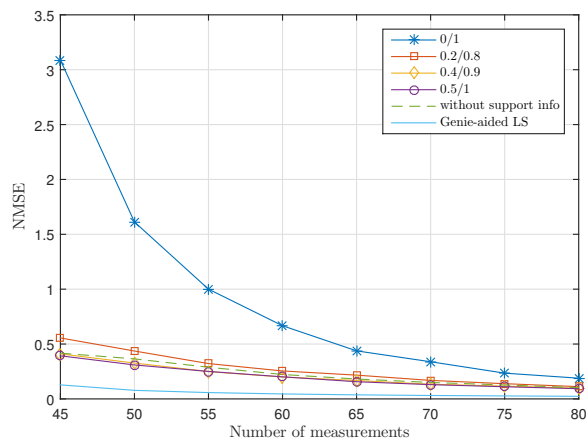


Figure 4.10: NMSE versus number of measurements with $M = 100$, $s = 37$, $\hat{s} = 40$, $a = 0.6$ and $\|\mathbf{e}\|_2 = 1$.

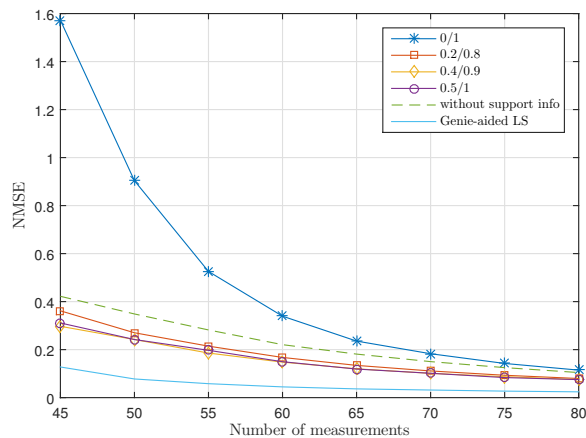


Figure 4.11: NMSE versus number of measurements with $M = 100$, $s = 37$, $\hat{s} = 40$, $a = 0.75$ and $\|\mathbf{e}\|_2 = 1$.

4.2. COMPARISON OF SIMPLE WEIGHTED ℓ_1 MINIMIZATION METHOD TO METHODS WITH DIFFERENT WEIGHTS

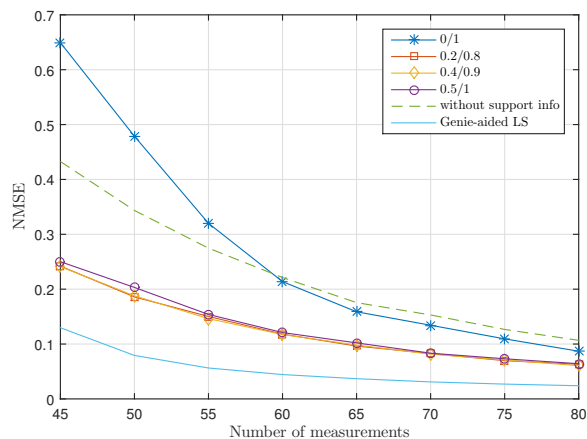


Figure 4.12: NMSE versus number of measurements with $M = 100$, $s = 37$, $\hat{s} = 40$, $a = 0.85$ and $\|\mathbf{e}\|_2 = 1$.

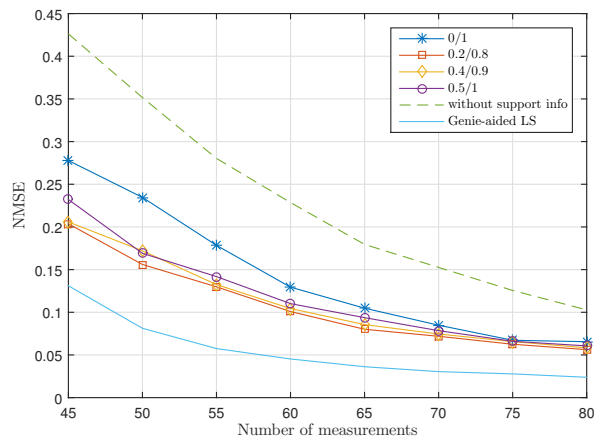


Figure 4.13: NMSE versus number of measurements with $M = 100$, $s = 37$, $\hat{s} = 40$, $a = 0.9$ and $\|\mathbf{e}\|_2 = 1$.

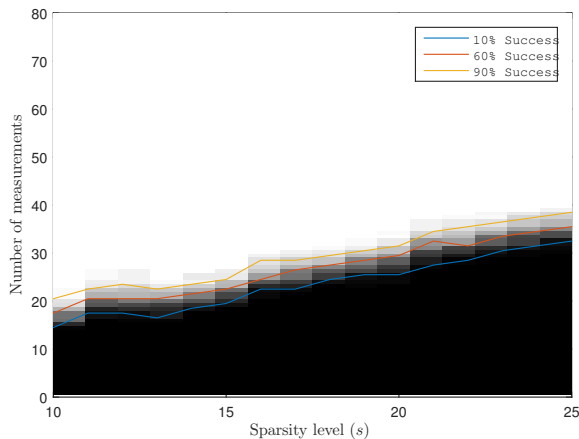


Figure 4.14: Phase Transition with $M = 100$, $\hat{s} = 10$, $a = 0.8$ and $\|\mathbf{e}\|_2 = 0$.

4.3 Phase Transitions

In Figures 4.14 and 4.15, we estimate the probability of success of the weighted ℓ_1 minimization method given the sparsity s of channel vector and the number of measurements N .

In Figure 4.14, we examine a noise free case with number of antennas at the BS $M = 100$, $\hat{s} = 10$, and accuracy of prior knowledge $a = 0.8$. We have success if $\|\hat{\mathbf{h}}^{\mathbf{a}} - \mathbf{h}^{\mathbf{a}}\|_2 \leq 10^{-4}$.

Figure 4.15 shows the Phase Transitions when there is additive noise. We set $M = 128$, $\hat{s} = 10$ and $a = 0.8$. Noise \mathbf{e} is random but with fixed norm $\|\mathbf{e}\|_2 = 10^{-3}$. Robust recovery is achieved when $\|\hat{\mathbf{h}}^{\mathbf{a}} - \mathbf{h}^{\mathbf{a}}\|_2 \leq 0.2$.

The brightness of each pixel (N, s) determines the empirical probability of success (i.e. black for 0% and white for 100%). For each pixel, we conduct 100 Monte Carlo experiments. Also, we plot the 10%, 60% and 90% curves of success probability, occurring from the data. Phase Transitions specify how the length of training symbols is changing to reach a certain percentage of success probability. In both cases, we observe that channel recovery could be achieved with low training overhead. Also, the width of the required measurements from failure to success (0%-100%), for a fixed s , is small.

4.3. PHASE TRANSITIONS

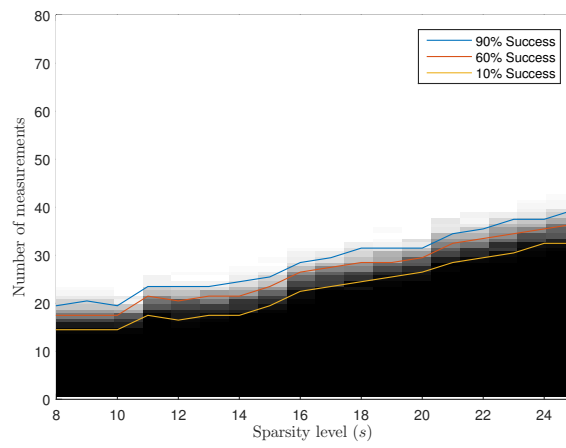


Figure 4.15: Phase Transition with $M = 128$, $\hat{s} = 10$, $a = 0.8$ and $\|\mathbf{e}\|_2 = 10^{-3}$.

Chapter 5

Conclusions & Future work

5.1 Conclusions

In this thesis, we study how to achieve reduction of the training overhead, exploiting the sparsity of Massive MIMO channels. Weighted ℓ_1 minimization using partial support information is suggested if the accuracy of prior information is high. In case of low accuracy, weighted ℓ_1 minimization exploiting partial support information does not offer any benefit. Our proposal, the weighted ℓ_1 minimization with different weights, would have better performance than the standard method with no perfect quality of prior knowledge. However, if the accuracy is high enough, then simple weighted ℓ_1 minimization should be preferred. Finally, Phase Transitions provide information about the number of measurements is needed to achieve channel recovery given the sparsity level s .

5.2 Future work

As future work, we could provide strict bounds about the required number of training symbols to achieve a certain quality of channel estimation by the proposed methods. Moreover, we could optimize the selection of the weights based on the accuracy of support estimate.

Appendix A

Proof of Equation (2.29)

$$\mathbf{e}_r^*(\Omega_{r1})\mathbf{e}_r(\Omega_{r2}) = \frac{1}{n_r} \sum_{k=0}^{n_r-1} (\exp(-j2\pi k\Delta_r\Omega_{r1}))^* \cdot \exp(-j2\pi k\Delta_r\Omega_{r2}) \quad (\text{A.1})$$

$$= \frac{1}{n_r} \sum_{k=0}^{n_r-1} \exp(j2\pi k\Delta_r\Omega_{r1}) \cdot \exp(-j2\pi k\Delta_r\Omega_{r2}) \quad (\text{A.2})$$

$$= \frac{1}{n_r} \sum_{k=0}^{n_r-1} \exp(-j2\pi k\Delta_r(\Omega_{r2} - \Omega_{r1})) \quad (\text{A.3})$$

$$= \frac{1}{n_r} \sum_{k=0}^{n_r-1} \exp(-j2\pi k\Delta_r\Omega_r) \quad (\text{A.4})$$

$$= \frac{1}{n_r} \frac{1 - \exp(-j2\pi n_r\Delta_r\Omega_r)}{1 - \exp(-j2\pi\Delta_r\Omega_r)} \quad (\text{A.5})$$

$$= \frac{1}{n_r} \frac{\exp(-j\pi n_r\Delta_r\Omega_r)}{\exp(-j\pi\Delta_r\Omega_r)} \cdot \frac{\exp(j\pi n_r\Delta_r\Omega_r) - \exp(-j\pi n_r\Delta_r\Omega_r)}{\exp(j\pi\Delta_r\Omega_r) - \exp(-j\pi\Delta_r\Omega_r)} \quad (\text{A.6})$$

$$= \frac{1}{n_r} \exp(-j\pi(n_r - 1)\Delta_r\Omega_r) \cdot \frac{j2 \sin(\pi n_r\Delta_r\Omega_r)}{j2 \sin(\pi\Delta_r\Omega_r)} \quad (\text{A.7})$$

$$= \frac{1}{n_r} \exp(-j\pi(n_r - 1)\Delta_r\Omega_r) \cdot \frac{\sin(\pi L_r\Omega_r)}{\sin(\pi L_r\Omega_r/n_r)}. \quad (\text{A.8})$$

Bibliography

- [1] E. G. Larsson, O. Edfors, F. Tufvesson and T. L. Marzetta, "Massive MIMO for next generation wireless systems," in *IEEE Communications Magazine*, vol. 52, no. 2, pp. 186-195, Feb. 2014
- [2] J. Shen, J. Zhang, K. Chen and K. B. Letaief, "High-Dimensional CSI Acquisition in Massive MIMO: Sparsity-Inspired Approaches," in *IEEE Systems Journal*, vol. 11, no. 1, pp. 32-40, March 2017
- [3] J. Shen, J. Zhang, E. Alsusa and K. B. Letaief, "Compressed CSI Acquisition in FDD Massive MIMO: How Much Training is Needed?," in *IEEE Transactions on Wireless Communications*, vol. 15, no. 6, pp. 4145-4156, June 2016
- [4] D. Tse and P. Viswanath, *Fundamentals of Wireless Communication*. Cambridge, U.K.: Cambridge Univ. Press, 2005.
- [5] Athanasios P. Liavas, *Lecture Notes on Wireless Communications*. Technical University of Crete, 2019.
- [6] X. Rao and V. K. N. Lau, "Distributed Compressive CSIT Estimation and Feedback for FDD Multi-User Massive MIMO Systems," in *IEEE Transactions on Signal Processing*, vol. 62, no. 12, pp. 3261-3271, June 2014
- [7] P. Kyritsi, D. C. Cox, R. A. Valenzuela and P. W. Wolniansky, "Correlation analysis based on MIMO channel measurements in an indoor environment," in *IEEE Journal on Selected Areas in Communications*, vol. 21, no. 5, pp. 713-720, June 2003
- [8] F. Kaltenberger, D. Gesbert, R. Knopp and M. Kountouris, "Correlation and capacity of measured multi-user MIMO channels," *2008 IEEE 19th International Symposium on Personal, Indoor and Mobile Radio Communications*, 2008, pp. 1-5
- [9] Y. Zhou, M. Herdin, A. M. Sayeed and E. Bonek, "Experimental study of MIMO channel statistics and capacity via the virtual channel representation", Feb. 2007
- [10] Michael Grant and Stephen Boyd. CVX: Matlab software for disciplined convex programming, version 2.1 <http://cvxr.com/cvx>, March 2014